Magnetic versus crystallographic fabrics in a basaltic lava flow

Jerôme Bascou, Pierre Camps, Jean-Marie Dautria

Available online at www.sciencedirect.com
SCIENCE DIRECT
Journal of Volcanology and Geothermal Research 145 (2005) 119–135
Journal of volcanology and geothermal research
www.elsevier.com/locate/jvolgeores

Magnetic versus crystallographic fabrics in a basaltic lava flow

Jérôme Bascou*, Pierre Camps, Jean Marie Dautria

Laboratoire de Tectonophysique, CNRS UMR 5568, Université de Montpellier II, Place E. Bataillon 34095 Montpellier cedex 5, France

Received 23 March 2004; received in revised form 6 December 2004; accepted 17 January 2005

Abstract

Combined anisotropy of magnetic susceptibility (AMS) and crystallographic studies were performed within a quaternary lava flow, for which we have a thorough knowledge of the flow direction. Microscope examinations, microprobe analyses and studies of rock magnetic properties show that AMS is carried by homogeneous multidomain Ti-rich titanomagnetite ($x \approx 0.6$). This mineral, forming either subhedral isolate individuals or grouped in various elongated aggregates, represents a late crystallized interstitial phase. AMS determined from samples collected in the lower, the middle and the upper part of the flow is characterized by a well-defined magnetic foliation whereas magnetic lineation is generally poorly grouped and therefore meaningless. The foliation plane of the lower and upper part of the flow show an obliquity, which is interpreted as an opposite imbrication indicating a westward flow in agreements with the known flow direction. In the lower part of the lava flow, the tight correlation between AMS and plagioclase lattice preferred orientation suggests that a silicate framework control the titanomagnetite crystallization and thus the orientation of the AMS ellipsoid.

Keywords: anisotropy; lava flow; magnetic susceptibility; crystallographic preferred orientation

1. Introduction

Petrological structures such as foliation and lineation due to the movement of lava flow during its emplacement are often difficult to observe and measure. To overcome this difficulty, the anisotropy of magnetic susceptibility (AMS) can be used. According to some studies on lava flows (Cañón-Tapia et al., 1996, 1997) and experimental results (Cañón-Tapia and Pinkerton, 2000), AMS might be related to the shear history of lava and might be used as a flow direction indicator in absence of other macroscopic evidences. An expected model is that the maximum of susceptibility axis $K1$ (the magnetic lineation) coincides to the flow direction while $K3$ (the pole of magnetic plane) is perpendicular to the surface of the lava flow. This normal fabric has been observed in many basaltic flows (Herrero-Bervera et al., 2002; Zhu et al., 2003). For high shear strains, experimental flow models (Arbaret et al., 1996; Ildefonse et al., 2002) show that the elongated particles interact and tend to

* Corresponding author. Actually at "Laboratoire Transferts Lithosphériques, CNRS UMR 6524, Université Jean Monnet, 23 rue du Dr Michelon 42023 Saint Etienne, France.
E-mail address: jerome.bascou@univ-st-etienne.fr (J. Bascou).

0377-0273/$ - see front matter © 2005 Elsevier B.V. All rights reserved.
doi:10.1016/j.jvolgeores.2005.01.007

align at low angle from the flow direction. Thus, AMS signature resulting from the imbricate fabric of elongated grains (Knight and Walker, 1988; Cañón-Tapia et al., 1996; Moreira et al., 1999; Geoffroy et al., 2002) should provide valuable information on the flow direction. However, several discrepancies between these models and AMS measurements have been reported. For highly magnetic rocks (such as basaltic lavas) in which AMS is principally carried by ferromagnetic minerals, various factors could complicate the interpretation of magnetic anisotropy such as (i) the presence of SD magnetite grains (or maghemite) with shape anisotropy leads to an "inverse susceptibility fabric" (Potter and Stephenson, 1988; Rochette et al., 1992, 1999); (ii) interactions between magnetite grains (Stephenson, 1994) due to an anisotropic distribution of ferromagnetic particles (Hargraves et al., 1991); (iii) variations of strain in a viscous magma (Dragoni et al., 1997); (iv) as well as post-flow alteration or tectonic stresses (Park et al., 1988).

The interpretation of susceptibility fabrics requires precise information about the magnetic mineralogy. Curie temperature and low-temperature susceptibility measurements inform on the nature of minerals carrying the magnetic susceptibility whereas hysteresis properties provide data on grain size and origin of magnetic anisotropy. Petrofabric studies and direct comparison between magnetic and crystallographic fabrics provide valuable constraints for the interpretation of the magnetic fabric (Benn et al., 1993; Yaouancq and MacLeod, 2000; Bascou et al., 2002). Such studies in volcanic rocks are quite scarce and mainly focused on the shape preferred orientation measurements of minerals (Ventura et al., 1996) and vesicles (Walker et al., 1999). Recent developments of the electron backscattered diffraction (EBSD) technique in the domain of Earth Sciences (Lloyd and Prior, 1999) have added a new possibility: the measurement of lattice preferred orientations for all minerals, with grain size <20 μm and a relative precision of crystal orientations better than 1° (Krieger Lassen, 1996).

In this paper, we present a crystallographic and AMS study of a basaltic lava for which the flow direction is known. Investigations on magnetic mineralogy, crystallographic preferred orientation of plagioclase, clinopyroxene and magnetite are combined. Magnetic and crystallographic fabrics are finally directly compared to the known flow direction of the lava.

2. Geological setting and sampling

Monts Ramus, located next to Saint Thibéry at 10 km northern Agde (southern France), are an alignment of three small cinder cones north–south oriented that erupted 0.7 Ma ago (K–Ar-dating method, Von Bonn and Heidelberg, 1965). Two basanitic flows are issued from the base of the major cone: the larger one (near 5 km^2) extends eastward and the other one (0.5 km^2) westward. This study is focused on the western flow (Fig. 1a) well exposed in an abandoned open quarry (42.38°N, 3.41°E) located about 100 m from the front of the flow. This flow has a total thickness of about 13 m. The slope during emplacement was undoubtedly very weak (<5°). Three structural parts can be distinguished on the outcrop (Fig. 1b): the lower is

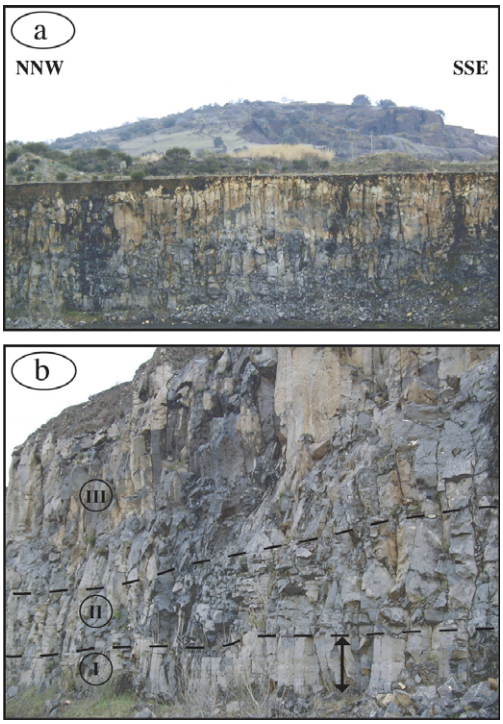

Fig. 1. (a) Outcrop of the Saint Thibéry lava flow in the open quarry. In the background the vent of the lava flow rises up; (b) the flow zones: (I) the lower colonnade, (II) the layered middle part and (III) the upper part of the flow (entablature). The height of the lower colonnade at the arrow location is about 1.5 m.

about 1.5 m thick and shows a structure of vertical columnar joints (lower colonnade); the middle part presents a variable thickness up to 3 m and displays sub-horizontal layered structures (layers between 10 and 30 cm); and the upper part (about 8 m) shows columnar joints irregular in shape and lightly sinuous (entablature). The bottom boundary of the flow is not visible and the total thickness of the flow is difficult to be precisely determined. From topographic considerations, the visible part of the flow base could represent from half to a third of the total thickness of the base. The flow is almost non-vesicular except close to the top boundary.

Systematic sampling of the base, the middle and the upper part of the lava flow has been carried out. Our strategy was to collect a minimum of 10 samples, according to a horizontal array, within the middle zone of each section in order to avoid particular border zone and some possible AMS variations that could be due, for example, by injection of lava pulses as describe by Cañón-Tapia and Coe (2002) in a flood basalt lava flow. At the base of the studied flow, samples were collected respecting a linear array at about 1 m below the boundary between the base and the middle part of the flow. Horizontal separation between samples ranges between 1.5 m and 9.5 m. Due to the thickness variability of the middle part of the flow, a minimum distance of 25 cm separates the sampling line from the two boundaries. In the upper part of the flow, the lower half zone is difficult to reach for drilling and samples were collected in the upper half zone at a minimum distance of 1 m of the top. Horizontal separation between samples mainly ranges between 1 and 3 m in accordance with the horizontal profile schema.

Cylinder cores of 2.5 cm in diameter were drilled using a gasoline-powered drill. They were oriented with respect to geographic north and horizontal plane using solar sightings and a magnetic compass equipped with a clinometer.

3. Mineralogy and rock magnetic study

Polished thin sections were prepared from specimens cut in the cylinder cores. Microscopic studies indicate a largely crystallized porphyritic lava (Fig. 2a). Phenocrysts of olivine and augite, about 20% of rock, are quite fractured and pluri-millimetric in size. Clinopyroxene displays the largest grains with prismatic forms. Olivine grains appear as granular and massive and inclusions of chromite are notified. Microcrysts are plagioclase, augite and iron–titanium oxides and the interstitial phases are nepheline and scarce glass. Plagioclase with labradorite composition (#An_{52}, microprobe analyses) forms the largest laths (50–100 μm in size) while the augite microliths are thin (about 20 μm). Microcrysts show variation of crystal content and size between the various parts of the flow. This is particularly clear for the laths of plagioclase that exhibit an increase in both size and total content in the lower and the upper part of the flow compared to the middle part. Reflected-light observations indicate that titanomagnetite is the principal opaque mineral representing about 5% of the lava volume;

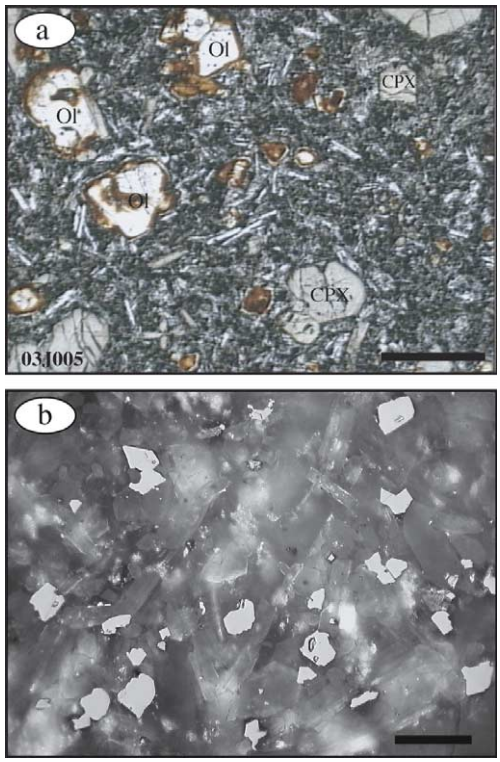

Fig. 2. Photomicrographs of thin section 03J005 from Saint Thibéry basalt. (a) Transmitted light photomicrograph showing characteristic micro-textures: phenocrysts of olivine (ol) and clinopyroxene (cpx); laths of plagioclase in white; titanomagnetite grains in black. Scale bar equals 200 μm; (b) reflected light photomicrograph showing titanomagnetite grains (white); oil immersion. Scale bar equals 30 μm.

the grains, mean size of 15 μm, are either subhedral isolate individuals or grouped in various elongated aggregates, apparently homogeneous, without any optical evidence of exsolution (Fig. 2b). Observations in thin section parallel to the flow plane show that the aggregates of titanomagnetite are generally sub-parallel to the elongated laths of plagioclase, although perpendicular orientation is also noticed. Microprobe analyses show that these oxides are Ti-rich titanomagnetites. Considering the conventional expression of titanomagnetite ($Fe_{3-x}Ti_xO_4$) with $0 \leq x \leq 1$, the analyses of samples from the upper and middle part of the flow give an ulvöspinel mole fraction (x) close to 0.6.

We carried out measurements of continuous thermomagnetic curves (K–T curves) at low and high temperature using a cryostat apparatus (CS-L) and a furnace (CS-3) under Ar atmosphere coupled to the KLY-3 Kappabridge instrument (Agico, Czech Republic). Representative K–T curves obtained on several specimens collected from each part of the lava flow are shown in Fig. 3. Low-temperature thermomagnetic curves are reversible and present characteristics similar to those of natural or synthetic samples containing multidomain homogeneous titanomagnetite with $x>0.3$ (Senanayake and Mc Elhinny, 1982). High-temperature curves are almost reversible. The steepest decrease in intensity of susceptibility is observed between 130–160 °C for sample 03J029 and 80–120 °C for samples 03J020 and 03J005 (Fig. 3). These relatively low Curie temperature ranges confirm that the magnetic carriers are mainly Ti-rich titanomagnetite (Nishitani, 1981; Dunlop and Özdemir, 1997). In the samples from the upper part of the flow (e.g., sample 03J029), the average Curie temperature is about 150 °C, which is in good agreement with the microprobe analyses of titanomagnetite giving $x \approx 0.6$ (O'Reilly, 1984). The lower Curie temperature obtained on the samples from the middle and the lower part of the flow (e.g., sample 03J005) could indicate the presence of titanomagnetite with $x>0.6$ and/or larger amount of Al and Mg in titanomagnetite with $x=0.6$. Some curves like those 03J029 and 03J020 (Fig. 3a,b) show a second decrease of the magnetic susceptibility around 420 °C and 480 °C, respectively, that could indicate the presence of metastable titanomaghemite corresponding to low-temperature oxidation of titanomagnetite.

Magnetization data calculated from partial hysteresis experiments known as first-order reversal curves (FORCs) are represented by contour plots of two-dimensional distribution function (Pike et al., 1999; Roberts et al., 2000) and are shown in Fig. 4. Hu is a measure of magnetostatic interactions while Hc provides indirect information about the magnetic domain structure. These measurements were performed on two samples from the lower (sample 03J005B) and the upper part (sample 03J029) of the flow using the Micro Vibrating Sample Magnetometer of the CEREGE Institute (Aix en Provence, France). Both full-size and high-resolution FORC diagrams are presented in Fig. 4. The contour distributions in our samples show different vertical and horizontal spreading. Pike et al. (1999) observed a correlation between the vertical spreading and the intensity of magnetostatic interactions for models of single-domain (SD) particle systems. The normal-resolution diagrams (Fig. 4, left side) display contours that diverge away from the origin. Such divergent patterns were interpreted by Roberts et al. (2000) as a manifestation of multidomain (MD) particles. The dissymmetry of contours is considered as characteristic of pseudo-single domain (PSD) grains while the convergence of the inner contours around a central peak (Fig. 4b, right) suggests a contribution of SD particles. Thus, the data point out a complex magnetic domain structure, a mixture of dominant large (MD) and fine magnetic grains (PSD±SD).

Finally, in order to have a complete description of rock magnetic properties, we checked the nature of the remanent magnetization carried by the ferromagnetic minerals. The Natural Remanent Magnetization (NRM) was measured using a JR-5A spinner magnetometer. Then, we averaged NRM directions and calculated statistical parameters assuming a Fisherian distribution. NRM directions are well clustered with a rather small value of the 95% confidence cone about the mean direction ($\alpha_{95}=1.9°$) and a large value of kappa ($k=220$), which is the precision parameter of Fisher distribution.

In order to check the presence of significant secondary components of magnetization, the 43 specimens used for AMS measurements were treated in zero field at 300 °C. Heating and cooling were performed under vacuum (better than 10^{-4} mbar) with the objective of reducing the probability

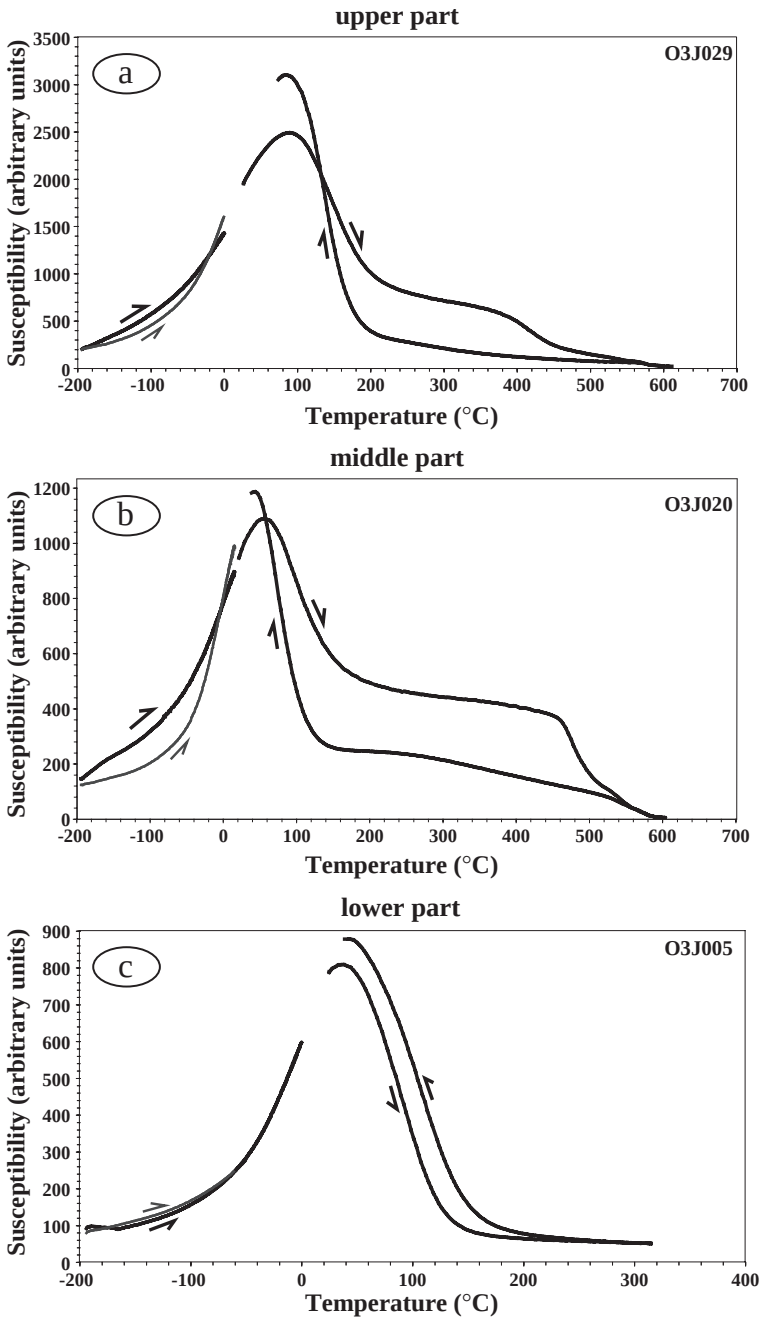

Fig. 3. Representative thermomagnetic curves at low and high temperature for samples from the upper part (a), the middle part (b) and the lower part of the flow (c). Measurements of thermal magnetic susceptibility changes are started and ended by heating from low temperature. The first heating is the thick black curve and the last heating is the fine grey curve.

of mineralogical changes, since they are usually due to oxidation. During this heating, the residual magnetic field was lower than 20 nT. On the average, about 60% of NRM were removed by this treatment. We did not observe any significant changes in the mean remanence direction (declina-

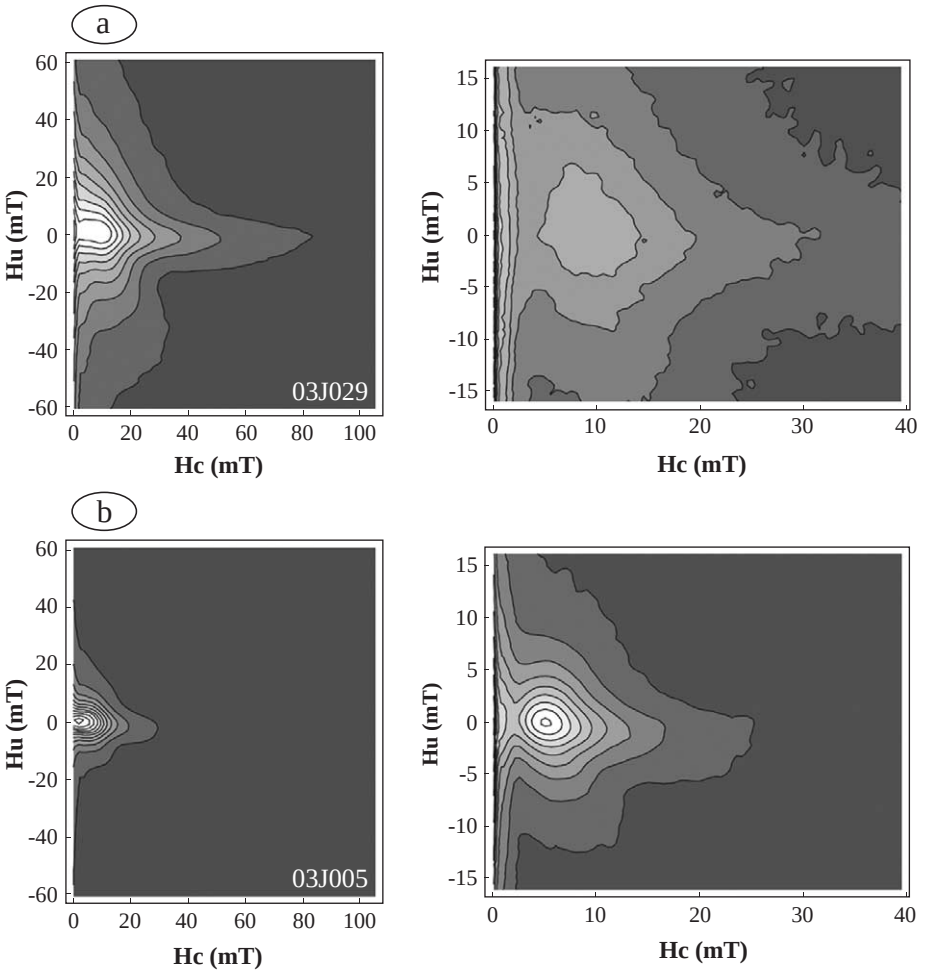

Fig. 4. Regular (left) and high (right)-resolution FORC diagrams for samples from the upper part (a) and the lower part of the flow (b). Smoothing factor, SF=3.

tion 349.3°, inclination 61.1°, α_{95}=1.6°). We concluded that no strong secondary magnetizations were present, as for example a piezoremanent magnetization that could have been acquired during quarry working. Furthermore, both the similarity between the NRM direction before and after the thermal treatment and the very low directional scatter (kappa 238) suggest that the NRM corresponds essentially to the primary Thermo-remanent Magnetization (TRM) acquired during the flow cooling. As expected from the radiochronologic age of this lava flow (0.7 Ma), the mean direction (declination 348°, inclination 59°) corresponds to a geomagnetic field of normal polarity.

4. Anisotropy of magnetic susceptibility and magnetic fabric

The anisotropy of magnetic susceptibility was measured on 2.2-cm long specimens cut from the oriented cylinder cores using KLY-3S Kappabridge. The sensitivity of this instrument under optimal conditions is 2×10^{-8} SI. The AMS measurements are described by a second-order tensor with three principal eigenvectors $K1\geq K2\geq K3$ (Tarling and Hrouda, 1993). We used the following AMS parameters: the mean susceptibility, Km=($K1$+$K2$+$K3$)/3; the corrected degree of anisotropy, P'=exp $\sqrt{\{2[(\eta_1-\eta)^2+(\eta_2-\eta)^2+(\eta_3-\eta)^2)]\}}$ with $\eta=(\eta_1+\eta_2+\eta_3)/3$,

η_1=log$K$1, η_2=log$K$2 and η_3 =log$K$3 (Jelinek, 1981). The ellipticity of the susceptibility ellipsoid was expressed by the shape parameter T (Jelinek, 1981) defined by: $T=(2\eta_2-\eta_1-\eta_3)/(\eta_1-\eta_3)$. $T>0$ for oblate magnetic susceptibility ellipsoids, and $T<0$ for prolate magnetic susceptibility ellipsoids. The principal eigen-

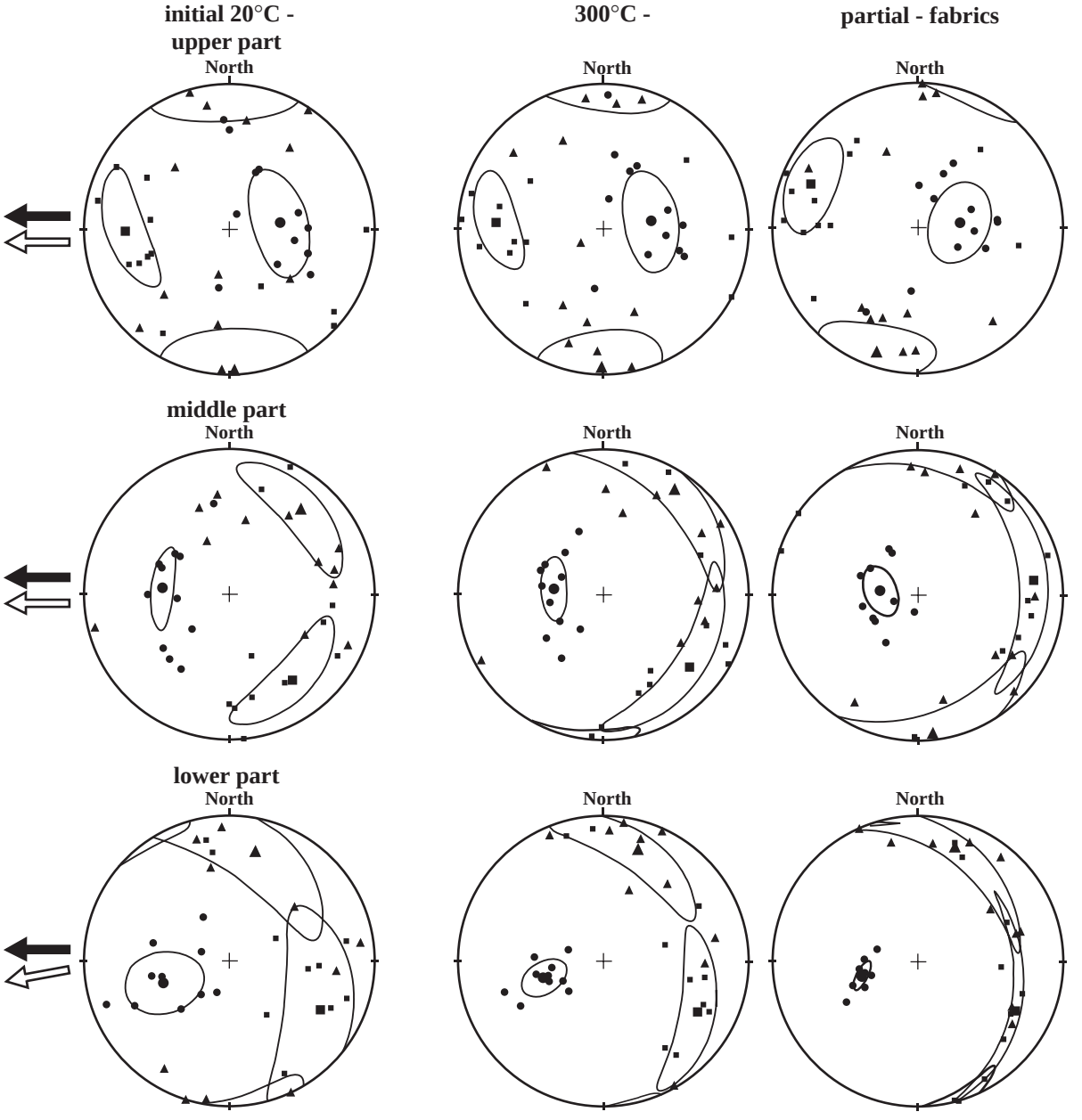

Fig. 5. AMS fabrics for the various zones of the Saint Thibéry lava flow. Initial AMS fabrics obtained at ambient temperature (left), after demagnetization at 300 °C (centre) and partial magnetic fabrics (right) obtained by tensor difference (Henry et al., 2003). The black arrows indicate the known lava flow azimuth and the white arrow indicate the inferred flow direction from magnetic fabrics. Squares = K1, maximum susceptibility axes, triangles = K2, intermediate susceptibility axes and circles = K3, minimum susceptibility axes. The confidence ellipses are computed from Jelinek's statistics (Jelinek, 1978). Equal-area diagrams, lower hemisphere projections, in the geographical horizontal plane.

vectors ($K1$, $K2$ and $K3$) of the mean normalized tensor and their confidence areas were calculated using the Jelinek method (Jelinek, 1978). AMS fabrics are shown in Fig. 5 and AMS parameters are listed in Table 1.

In order to check possible interactions between remanence and AMS (Rochette et al., 1992), we also measured the magnetic fabric after removing most of NRM (60%) by thermal demagnetization under vacuum at 300 °C (Fig. 5). The directions of the mean principal axes do not differ significantly before and after partial NRM removal but they tend to be better defined, some ellipses becoming slightly smaller after thermal treatment. The change in magnetic fabric after heating may be due to the disappearance of a small NRM-dependant AMS while some physical and/or chemical changes in magnetic mineralogy may be the cause of the increase in mean susceptibility (from 3.06 to 3.84 10^{-2} SI after treatment, Table 1). New approach leading to isolate the partial magnetic fabric that appears or disappears during thermal treatment (Henry et al., 2003) was applied in samples. The fabrics obtained by tensor difference are shown in Fig. 5 (right diagrams). These fabrics are more homogenous that initial fabric suggesting that the initial fabrics are composite. However, all AMS fabrics before and after partial demagnetization as well as partial isolated fabric roughly present similar characteristics (concentration and orientation of $K3$ axes, shape of the ellipsoid given by the T parameter, see Table 1) that highlight the robustness of flow direction inferred from initial AMS data.

The mean bulk susceptibility ranges from 2.10^{-2} SI in the lowest part to 4.10^{-2} SI in the uppermost part of the lava flow. The main bulk susceptibility is essentially due to large titanomagnetite grains that represent ~5% in volume of rock. The anisotropy ratios are quite low P' values are less than 0.01. Ellipsoids are all oblate ($0.313 \leq T \leq 0.614$). The decrease of P' and T expresses a decrease of the anisotropy and the ellipsoid flatness from the lowest to the uppermost layers. This could reflect the effect of settling by gravity. The increase of an oblate (and anisotropic) ellipsoid with increase depth has been also related to the effect of a more pronounced shear at the base of the flow (see experimental results of Cañón-Tapia and Pinkerton, 2000).

The magnetic susceptibility axes $K1$ and $K2$ are relatively spread within both lower and middle part of the flow and tend to form large girdles close to the horizontal plane (Fig. 5). Moreover $K1$ and $K2$ are sometimes permuted and thus the distribution of the magnetic axes $K1$ cannot be taken as a reliable indicator of the flow direction. However, we note that in the upper part of the flow, the magnetic lineation $K1$ fits well with the known flow direction. On the other hand, all samples show rather well concentrated $K3$ axes with similar mean direction at about 35° from

Table 1
AMS data

Sites	n	Km (10^{-2} SI)	$K1$ mean (Az./Incl.)	$K2$ mean (Az./Incl.)	$K3$ mean (Az./Incl.)	AMS parameters	
						P'	T
Before thermal treatment							
STB3	12	3.39	270°/29°	178°/03°	82°/61°	1.002	0.312
STB2	11	3.20	144°/28°	40°/24°	275/51°	1.008	0.510
STB1	10	2.60	118°/30°	13°/23°	252°/50°	1.010	0.615
After thermal treatment at 300 °C							
STB3	12	4.03	274°/27°	181°/5°	81°/63°	1.010	0.342
STB2	11	4.02	130°/24°	34°/14°	277°/62°	1.012	0.818
STB1	10	3.48	118°/27°	17°/21°	255°/55°	1.017	0.775
Partial magnetic fabric data							
STB3	12	0.64	293°/21°	198°/11°	83°/66°	1.026	0.303
STB2	11	0.82	82°/21°	174°/5°	277°/69°	1.039	0.809
STB1	10	0.88	117°/26°	18°/19°	256°/57°	1.042	0.900

n = Number of specimens measured. The mean susceptibility Km, the magnetic anisotropy P' and the shape parameter T are defined in the text.

vertical. Averaged $K3$ axes point westward in the lower and the middle part of the flow and eastward in the upper part, which indicates opposite magnetic imbrications. In dikes opposite imbrications observed when approaching the margins are used to determine the magmatic flow direction (Moreira et al., 1999; Geoffroy et al., 2002). Consequently, in the Saint Thibéry case, AMS measurements indicate a westward flow direction in agreement with that deduce from the flow morphology and the location of the eruptive vent.

5. EBSD-measured Lattice Preferred Orientations

Measurements of lattice preferred orientation (LPO) of plagioclase, clinopyroxene and titanomagnetite were performed via the analysis of electron backscattered diffraction (EBSD) images using a scanning electron microscope JEOL 5600-SEM. For EBSD analyses, the thin sections obtained from oriented cylindrical specimens are tilted at 70° from the horizontal within the SEM chamber. An optimum quality of diffraction images was obtained with free coating and carefully polished samples. Typical experimental conditions were 18 kV for accelerating voltage, 30 μA for current intensity and 40 mm for the working distance. Diffraction patterns collected from each grain were indexed using the CHANNEL5+ software of HKL technology (Schmidt and Olesen, 1989). At each point of measurement the Euler angles ($\varphi 1$, θ, $\varphi 2$) characterizing the 3D orientation of the crystal lattice were determined with a precision better than 1° (Krieger Lassen, 1996). Due to the large contrast in mean atomic number between silicate phases (plagioclase, augite) and titanomagnetite, automatic orientation mapping was not possible and the crystallographic orientations were measured grain-per-grain on the whole surface of the thin sections. For titanomagnetite, indexation of diffraction images and projection of crystallographic orientations in density diagrams (Fig. 6) are based on crystallographic data (Laüe group, unit cell parameters, atoms positions within the unit cell) given by Wechsler et al. (1984). For plagioclase (labradorite, as indicated by our microprobe analyses), and for clinopyroxene (augite), we used the crystallographic parameters of Wenk et al. (1980) and Bertolo et al. (1994), respectively. An excellent indexation quality, marked by a Mean Angular Deviation (MAD) generally lower than 0.6°, was obtained using these crystallographic data files.

The measured LPO of these three minerals (plagioclase, clinopyroxene, titanomagnetite) are presented on equal area, lower hemisphere projection in the specimen reference frame (Fig. 6). For plagioclase, maximum density directions are equally presented in the geographical frame (Fig. 7). Between 151 and 314 crystallographic orientations were determined per sample and the density contours are expressed in multiple uniform distribution (mud). The fabric strength is expressed by the dimensionless texture J index (Bunge, 1982), which equals to unity for a random distribution and tends towards infinity for a single crystal.

Plagioclase LPO from all samples is characterized by a strong concentration of (010)-poles, corresponding to the most developed crystallographic planes. The two others (100) and (001)-poles, although less concentrated, are still well clustered. The projections in the geographic referential frame (Fig. 7) show that the plane (010) is almost horizontal in the middle part (sample 03J016), moderately dipping (35°) in the lower part and more strongly dipping (45°) in the upper part of the flow. In the lower and upper part of the flow, the (100)-poles, which are almost parallel to the crystallographic [100]-axes, are preferentially oriented in the east–west flow direction. These observations agree quite well with known plagioclase fabrics in magmatically deformed gabbroic rocks for which the preferred orientation of (010) planes corresponds to the foliation and the preferred orientation of [100]-axes is parallel to the lineation (Yaouancq and MacLeod, 2000; Ildefonse et al., 2002). The highest fabric strength (J index >5) is obtained for the samples from the upper and the lower part of the flow (Fig. 6a), with a maximum value of J (5.46) in the lower zone. The samples collected from the middle part have a J index reduced to 4.

Clinopyroxene LPO is less concentrated than plagioclase LPO. However, the crystallographic planes of these two minerals show close relationships: (001)-clinopyroxene tend to be parallel to (100)-plagioclase, (100)-clinopyroxene tend to be parallel to (010)-plagioclase and in the upper part of the flow (010)-clinopyroxene are nearly parallel to (001)-plagioclase. Thus, it is obvious that these minerals, which constitute

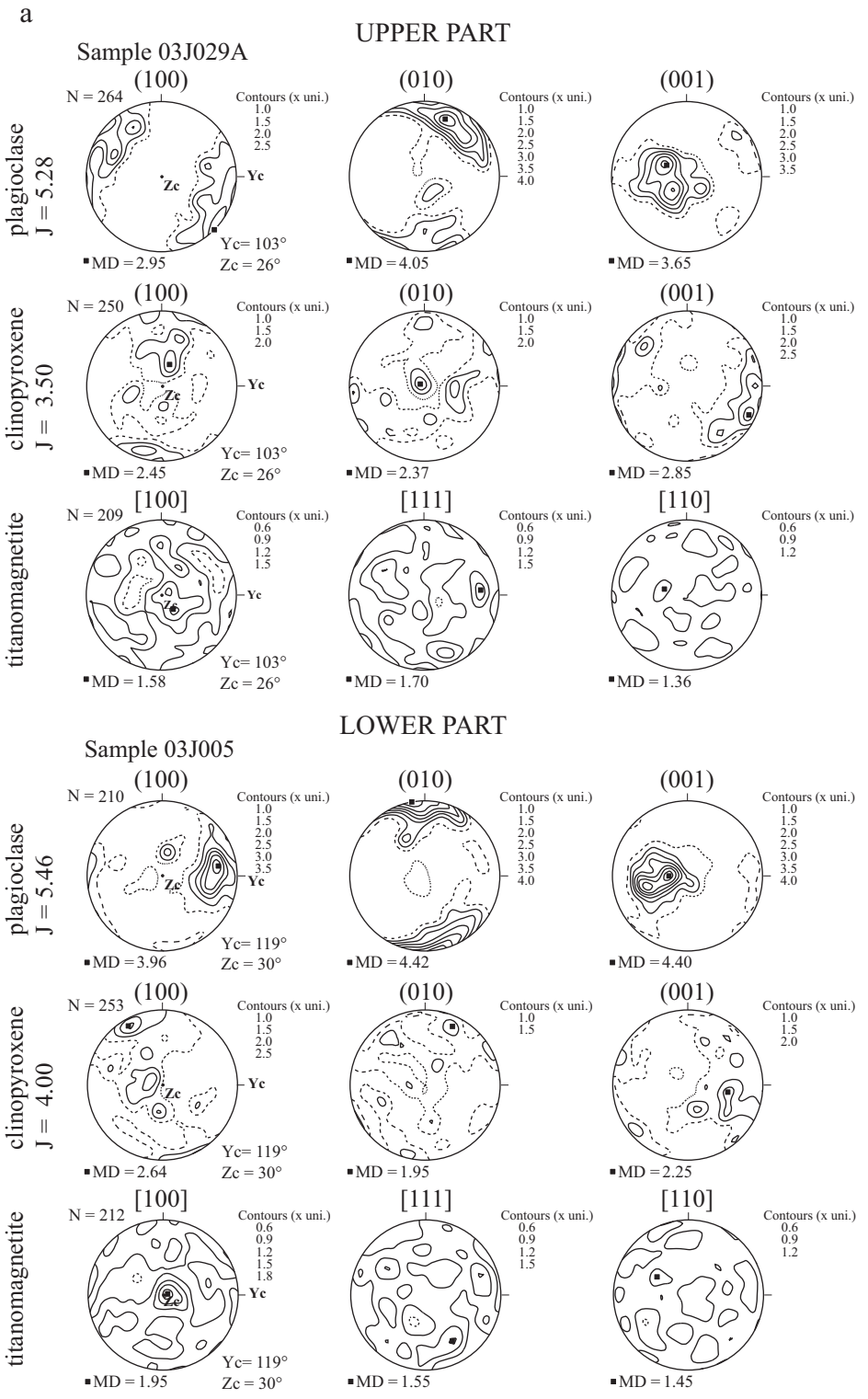
a
UPPER PART
Sample 03J029A
plagioclase J = 5.28
clinopyroxene J = 3.50
titanomagnetite
(100)
(010)
(001)
[100]
[111]
[110]
N = 264
N = 250
N = 209
Contours (x uni.)
Zc
Yc
Yc= 103°
Zc = 26°
MD = 2.95
MD = 4.05
MD = 3.65
MD = 2.45
MD = 2.37
MD = 2.85
MD = 1.58
MD = 1.70
MD = 1.36
LOWER PART
Sample 03J005
plagioclase J = 5.46
clinopyroxene J = 4.00
N = 210
N = 253
N = 212
Yc= 119°
Zc = 30°
MD = 3.96
MD = 4.42
MD = 4.40
MD = 2.64
MD = 1.95
MD = 2.25
MD = 1.95
MD = 1.55
MD = 1.45

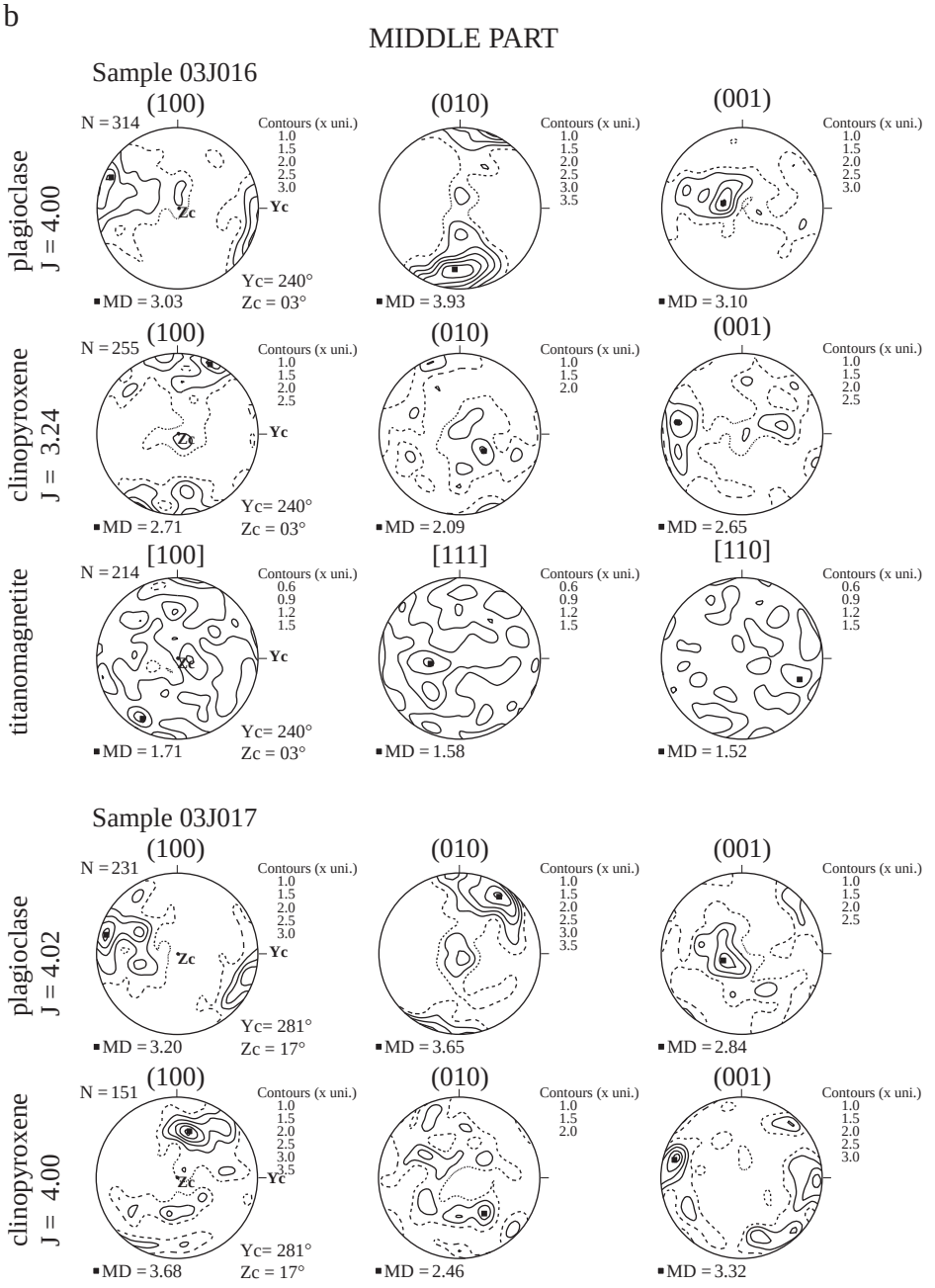

Fig. 6. Lattice Preferred Orientation of plagioclase, clinopyroxene and titanomagnetite of samples from the lower and the upper part (a), and the middle part (b) of the flow. Equal area projection in the lower hemisphere and in the specimen coordinate system with Yc the specimen azimuth and Zc the dip of the drilled core (Zc=90° for a vertical core). Contours are in Multiples of Uniform Distribution (M.U.D). *J* is the texture index and *N* the number of measurements.

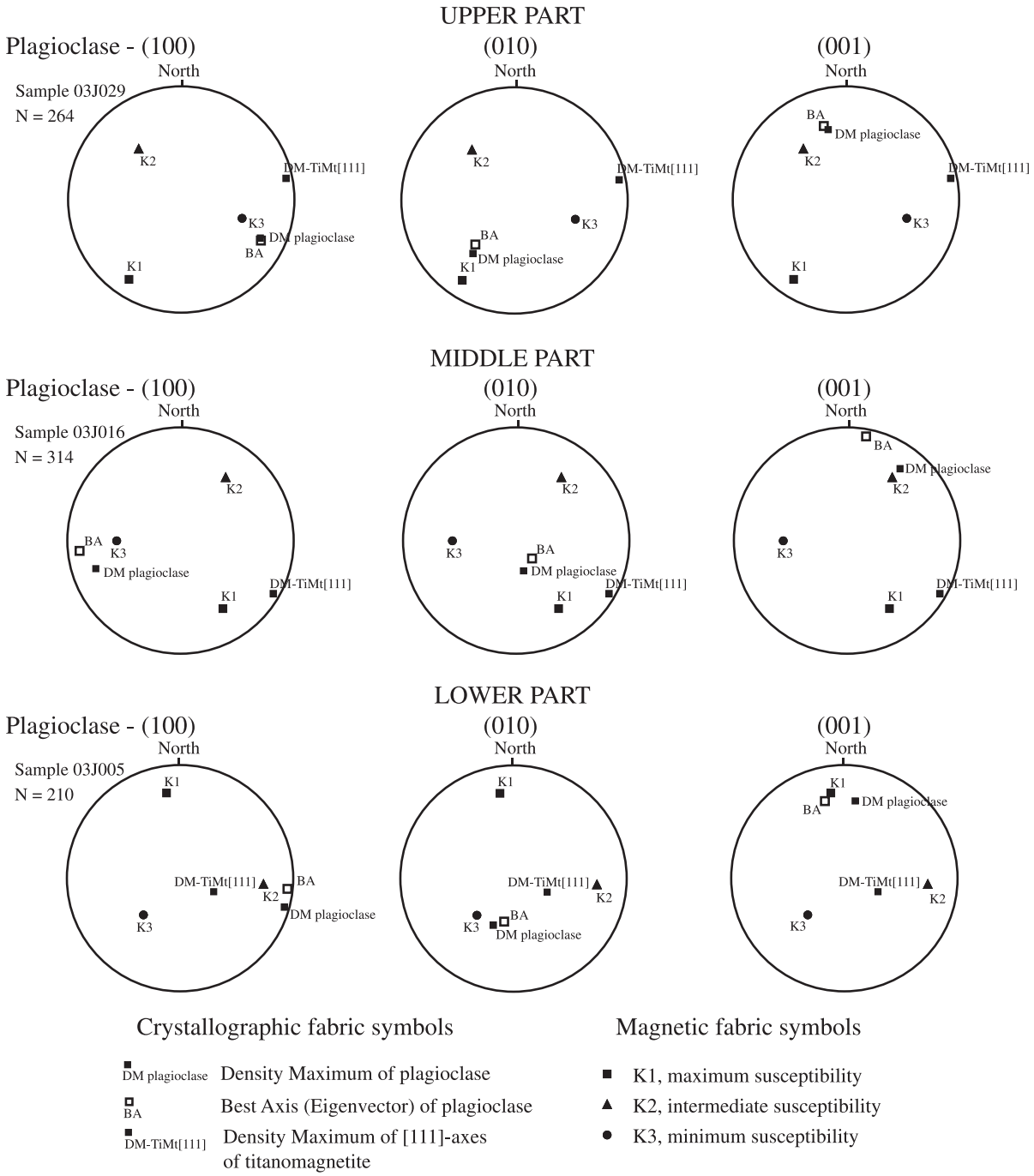

Fig. 7. Density maximum and the "Best Axis" (eigenvector) of plagioclase LPO of samples from the various parts of the flow in the geographical horizontal plane. The density maximum of (100)-poles and [111]-axes of titanomagnetite, and the mean eigenvectors (*K*1, *K*2 and *K*3) are also plotted. *N* is the number of measurements.

more than 65% of the modal content of the lava, present similar flow-related preferred orientations.

Titanomagnetite LPO is very weak in all samples. However, we observe a well-defined maximum of concentration (DM=2 mud) of [100] equivalent axes (Fig. 6a) for the sample collected in the lower zone of the flow. This maximum lays within the foliation plane defined by the (010) planes of plagioclase and is located close to the Density Maximum of plagioclase (001)-poles.

6. Discussion

6.1. Comparison between magnetic and crystallographic fabrics

An image analysis was performed in order to control the coaxiality between the titanomagnetite subfabric (aggregate elongation and subsidiary, shape preferred orientation of individual grains) and the magnetic fabric (Fig. 8). In four representative specimens collected in the different parts of the flow, image analysis was carried out on three thin sections cut parallel to the references (*K*1, *K*3), (*K*2, *K*3) and (*K*1, *K*2)-planes of the magnetic susceptibility ellipsoid. The sections were digitized and processed in order to bring out the subfabric of Fe–Ti oxide minerals. In each section, the shape fabric was extracted using the intercept method of Launeau and Robin (1996) (see http://www.sciences.univ-nantes.fr/geol/UMR6112/SPO/index.html), which is based on analysis of boundary orientation distribution of objects. Comparison between the shape fabric ellipses and the AMS ellipses (Fig. 8b) shows angular departures between the long and short axes of the shape orientation ellipse and the *K*1, *K*2 and *K*3 axes of the AMS ellipsoid are less than 20°. Theses results confirm that the magnetic fabric can be equated to the titanomagnetite subfabric.

In order to facilitate comparisons between magnetic and crystallographic fabrics, both magnetic and crystallographic data for all samples were plotted in geographic coordinates (Fig. 7). Moreover, to compare LPO with the principal mean susceptibility axes, the eigenvalues and eigenvectors of normalized orientation tensors (Woodcock and Naylor, 1983) were calculated

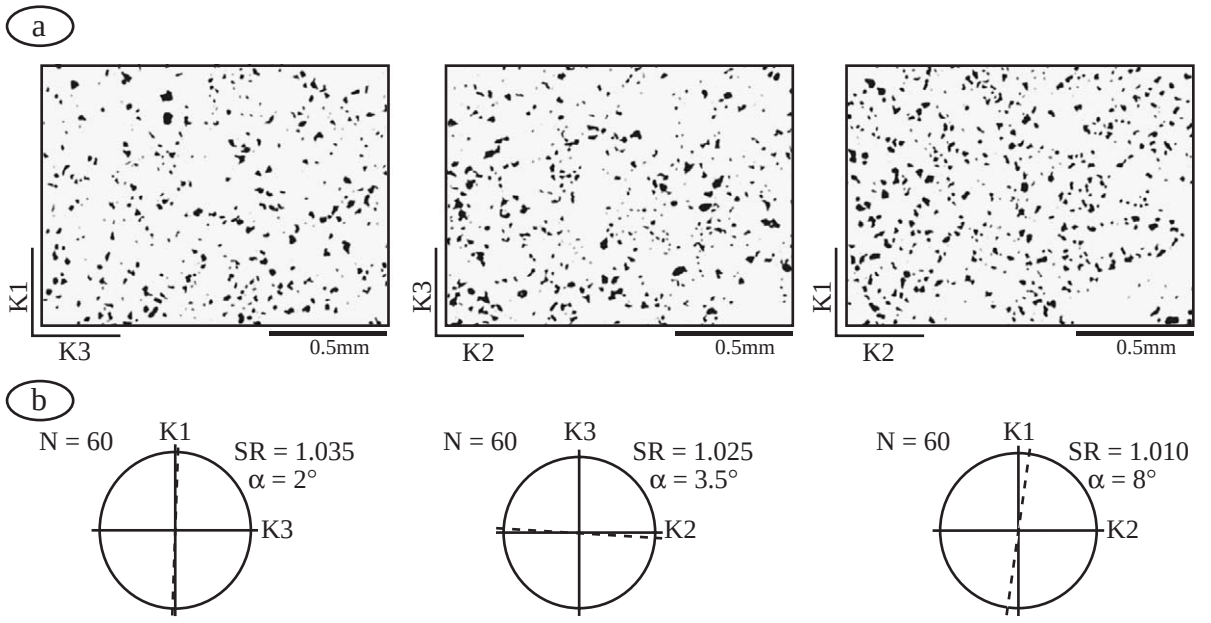

Fig. 8. Image analysis of Fe–Ti oxides for sample O3JOO5. (a) Three perpendicular sections were cut parallel to the *K*1*K*3, *K*2*K*3 and *K*1*K*2 planes and digitized images (size: ~1.1 mm×1.4 mm) are filtered and cleaned to isolate the subfabric of the Fe–Ti oxide grains. (b) Shape fabric ellipses using the intercept method (Launeau and Robin, 1996) for the three section planes. *N* is the number of digitized images gathered for the image analysis in each section. SR is the shape ratio; α is angle between the long axis of the shape preferred orientation ellipse (dotted line) and the *K*1 and *K*2 axis of magnetic susceptibility.

from LPO. We plotted in Fig. 7 the "Best Axis" of plagioclase that corresponds to the eigenvector of the largest eigenvalue of normalized orientation tensors.

Relationships between AMS ellipsoid and LPO of plagioclases are different for samples collected from the different parts of the flow. These relationships are quite clear in the lower part (Fig. 7). For the sample collected in this zone, a tight correlation is observed between the AMS ellipsoid axes and the LPO of plagioclase: the $K1$ axis is sub-parallel to the Best Axis of (001) planes, the $K2$ axis is close to the Best Axis of (100) planes and the $K3$ axis is close to the maximum of concentration (Density Maximum and Best Axis) of (010)-poles. In the upper part of the flow, the $K1$ axis tends to be close to the maximum of concentration of (010)-poles, the $K2$ axis is close to the maximum of concentration of (001)-poles and the $K3$ axis is close to the maximum of concentration of (100)-poles.

We also plotted in Fig. 7 the Density Maximum of titanomagnetite [111]-axes. Despite a weak LPO, orientation of [111]-axes (which thus must be considered with caution) is of particular interest because this axis corresponds to the preferred magnetization axes (O'Reilly, 1984). However, there is no systematic correlation between the orientation of the Density Maximum of titanomagnetite [111]-axes and the $K1$ axis or the LPO of plagioclase.

6.2. Origin of the AMS

Magnetic anisotropy of rock-forming minerals can be of shape origin, magnetocristalline or magnetostrictive. A non-intrinsic origin, based on the interactions between magnetite grains due to an anisotropic distribution, has been also proposed by Hargraves et al. (1991). Later, several theoretical models and experiments have been done to better understand the effect of magnetic interactions between neighbouring grains (Stephenson, 1994; Grégoire et al., 1995, 1998; Cañón-Tapia, 1996, 2001; Gaillot et al., 2002). However, mostly due to the scarcity of detailed textural investigations, the role of magnetic interactions in AMS of natural rocks is still poorly constrained.

Shape anisotropy is negligible for magnetically weak minerals as silicates and could be only slightly expressed for Ti-rich titanomagnetite crystals found in the Saint Thibéry lava flow. In the absence of an obvious correlation between the preferred orientation of titanomagnetite [111]-axes and the principal magnetic susceptibility axes, magnetocristalline anisotropy can also be dismissed. Magnetostrictive anisotropy requires internal stress in crystals that should decrease with heating, but conservation of mean magnetic susceptibility directions after thermal demagnetization performed at 300 °C suggests that this origin should be also excluded. Thus, the anisotropy seems to be related to the spatial distribution of titanomagnetite grains.

Titanomagnetite grains, which represent 5% of the modal content of samples, are interstitial, usually subhedral, roughly equant, isolated individuals or grouped in aggregates. These observations suggest that the grains formed late in the crystallization history. In the contrary, the plagioclase and the largest clinopyroxene crystals are early crystallized. These minerals, which represent more than 65% of the rock modal volume, constitute a flow-oriented silicate framework constraining the spatial distribution of interstitial titanomagnetite. In the lower part of the flow, the tight relationship between AMS (carried by titanomagnetite) and the plagioclase LPO (itself coaxial to the clinopyroxene) suggests that such a silicate framework control the crystallization of titanomagnetite. The experimental studies of Hargraves et al. (1991) indicate that AMS can be issued from an anisotropy of distribution caused by a silicate "template". The same reason is also invoked by Wolff et al. (1989) as the principal factor of AMS in welded tuffs. More recently, Archanjo et al. (2002) have proposed that competition of interstitial magnetite grains crystallizing both along and perpendicular to the plagioclase lineation of mafic dikes could produce abnormal magnetic fabric. Processes of drag and collisions between adjacent grains within a viscous flow in movement could also result in the creation of openings and closings normal to the stretching direction (Launeau and Cruden, 1998). Thus, the occurrence of elongated aggregates of titanomagnetite perpendicularly to the plagioclase alignment could be favored. Such an anisotropic distribution might generate the orientation of the $K1$ axis perpendicular to the flow direction as observed in sample from the lower part of the flow (Fig. 7). The strong planar plagioclase and clinopyroxene fabric measured at the base of the flow could also facilitate the magnetic lineation ($K1$) perpendicular to the flow direction and the parallelism

between the crystallographic and magnetic foliation. In contrast, a lack of correlation is noticed for sample from the middle part and a surprising closeness is observed between the (010)-poles of plagioclase and $K1$ in the sample from the upper part of the flow. The very low shape magnetic parameter (T) characterizing the samples of the middle and the upper part of the flow (T=0.161 and T=−0.09, respectively) could privilege interchanges between the main principal K axes. It is interesting to note that the magnetic ellipsoid is closer to the plagioclase fabric in the upper part of the flow where the strain is higher than in the middle part.

6.3. Strain pattern and velocity profile of the flow constraint from LPO

Imbrication of the main susceptibility axes in opposed direction from the upper and lower part of the flow is commonly observed in natural lava flows. These opposite imbrications are interpreted as due to the velocity profile characteristic of the flow between the ground surface and a roof of solidified lava (Cañón-Tapia et al., 1996, 1997). During the cooling of the flow, the roof thickness increases and the vertical velocity profile evolves as a function of time. Modeling of strain within a lava flow (Merle, 1998, 2000) shows that for a sufficient thickness of the roof the sense of shear initially identical throughout the whole lava flow, will be reversed on both sides of a central zone of low strain where the flow reaches its highest velocity.

In the studied flow, the orientation of mean susceptibility axes is relatively similar in the lower and the middle zone. The planes of magnetic foliation are characterized by a consistent obliquity (~35°) interpreted to constitute an imbrication, opposite in sense to that defined in the upper part of the flow. Thus, one expects a zone of minimum shear located at the transition between the middle and the upper part. However, both field observations of horizontal layering and petrographic observations displaying the lowest crystal content do not agree with this interpretation. They rather suggest that the whole middle part of the flow does constitute the zone of the highest velocity.

Deformation at the magmatic state leads to the development of a crystallographic fabric defined by the alignment of anisometric crystals in a flowing matrix (Blumenfeld and Bouchez, 1988; Nicolas, 1992). This fabric characterizes the end of the deformation history of the lava flow. Analogue modeling of non-coaxial deformation in concentrated suspension of particles suggests that the fabric strength increases as a function of particles shape ratio and as a function of the finite strain (Ildefonse and Fernandez, 1988). Considering various assumptions such as initial random orientation of crystals and constant shape during the deformation, Ventura et al. (1996) use the distribution of crystal shape preferred orientation to estimate the shear strain in natural lava flow. This shear strain appears mainly localized in the outer margins of the flow, the central zone being characterized by lacks of well-defined crystal preferred orientation.

In the Saint Thibéry lava, samples from the lower and the upper part of the flow show similar strong strength fabric of plagioclase (J_{index}>5), higher than those measured in samples from the middle part (J_{index}=4). Thus, crystallographic fabrics suggest that the middle part of the flow represents a low shear strain zone. The observed variations of the fabric strength indicate a velocity gradient between the inner and the outer part, which characterizes the last deformation event. The similitude of fabric strength of samples collected in the middle zone agrees with the classical models of plug flow moving between two non-deformed side walls. In the future, more detailed and systematic crystallographic preferred orientation measurements could allow defining precisely the shape of the vertical velocity profile of the flow.

7. Conclusions

The main conclusions of this study can be summarized as follows:

1. Multidomain titanomagnetite (x=0.6) is the main provider of AMS in the Saint Thibéry lava. This mineral represents a late interstitial phase that crystallized in a silicate framework controlled by plagioclase. The crystallographic fabric is characterized by the strong concentration of (010) planes of plagioclase that define the foliation, together with the (100) planes of clinopyroxene.
2. Magnetic lineation is neither systematically clearly defined nor consistent with the known lava flow direction. Magnetic foliation is always well defined in the various parts of the flow. Obliquity of $K3$

axes in the upper and the lower part of the flow defines opposite imbrication that indicates the geologic westward flow direction.

3. Comparison at the sample scale between main susceptibility axes and plagioclase LPO shows a good agreement for the lower part of the flow. In particular, we note a significant parallelism between the crystallographic foliation and the magnetic foliation. The good fit between magnetic and crystallographic fabrics suggests that the AMS is constrained by the silicate framework. Discrepancies observed in the upper and the middle part of the flow underlines the necessity of more detailed investigations on growth processes of titanomagnetite in oriented multi-mineral aggregates and experiments on magnetic interactions. However, our observations suggest that the lower part of the flow is the most indicated region to obtain flow direction from AMS.
4. EBSD-measured crystallographic preferred orientation of silicate phases provides valuable, complementary information for determining the velocity profile of the flow and thus appears as an attractive tool to constrain the dynamic of the lava flow.

Acknowledgements

We thank Michel Prévot, Bernard Henry and two anonymous reviewers for their useful comments and suggestions. FORC analyses have been realized at the CEREGE, Aix en Provence (France). Pierre Rochette and Guillaume Plenier are gratefully acknowledged. We also thank Christophe Nevado for preparing the thin sections. LPO measurements were carried out with Laboratoire de Tectonophysique EBSD/SEM system funded by grants from CNRS/INSU, Université Montpellier II, ISTEEM and NSF #EAR-9526840 "Anatomy of an Archean craton".

References

Arbaret, L., Diot, H., Bouchez, J.L., 1996. Shape fabric of particles in low concentration suspensions: 2D analogue experiments and application to tiling in magma. J. Struct. Geol. 18, 941–950.

Archanjo, J.A., Araújo, M.G.S., Launeau, P., 2002. Fabric of the Rio Ceará-Mirim mafic dyke swarm (Northeastern Brazil), determined by anisotropy of magnetic susceptibility and image analysis. J. Geophys. Res. 107 (B3), 10.1029–11.1041.

Bascou, J., Raposo, M.I.B., Vauchez, A., Egydio-Silva, M., 2002. Titanohematite lattice preferred orientation and magnetic anisotropy in high-temperature mylonites. Earth Planet. Sci. Lett. 198, 77–92.

Benn, K., Rochette, P., Bouchez, J.L., Hattori, K., 1993. Magnetic susceptibility, magnetic mineralogy and magnetic fabrics in a late Archean granitoid–gneiss belt. Precambrian Res. 63, 59–81.

Bertolo, S., Nimis, P., Dal Negro, A., 1994. Low-Ca augite from experimental alkali basalt at 18 kbar: structural variation near the miscibility gap. Am. Mineral. 79, 668–674.

Blumenfeld, P., Bouchez, J.L., 1988. Shear criteria in granite and migmatite deformed in the magmatic and solid states. J. Struct. Geol. 10, 361–372.

Bunge, H.J., 1982. Texture Analysis in Materials Sciences. Butterworths, London. 593 pp.

Cañón-Tapia, E., 1996. Single-grain versus distribution anisotropy: a simple three-dimensional model. Phys. Earth Planet. Inter. 94, 117–131.

Cañón-Tapia, E., 2001. Factors affecting the relative importance of shape and distribution anisotropy in rocks: theory and experiments. Tectonophysics 340, 117–131.

Cañón-Tapia, E., Coe, R., 2002. Rock magnetic evidence of inflation of a flood basalt lava flow. Bull. Volcanol. 64, 289–302.

Cañón-Tapia, E., Pinkerton, H., 2000. The anisotropy of magnetic susceptibility of lava flows: an experimental approach. J. Volcanol. Geotherm. Res. 98, 219–233.

Cañón-Tapia, E., Walker, G.P.L., Herrero-Bervera, E., 1996. The internal structure of lava flows—insights from AMS measurements: I. Near-vent a'a. J. Volcanol. Geotherm. Res. 70, 21–36.

Cañón-Tapia, E., Walker, G.P.L., Herrero-Bervera, E., 1997. The internal structure of lava flows—insights from AMS measurements: II. Hawaiian pahoehoe, toothpaste lava and 'a'a. J. Volcanol. Geotherm. Res. 76, 19–46.

Dragoni, M., Lanza, R., Tallarico, A., 1997. Magnetic anisotropy produced by magma flow: theorical model and experimental data from Ferrar dolerite sills (Antarctica). Geophys. J. Int. 128, 230–240.

Dunlop, D.J., Özdemir, Ö., 1997. Rock Magnetism: Fundamentals and Fontiers. Cambridge Univ. Press, Cambridge. 573 pp.

Gaillot, P., de Saint Blanquat, M., Bouchez, J.L., 2002. Numerical modelling of magnetic susceptibility in ferromagnetic rocks: the role of magnetic interactions. Geological Society of America Meeting, Denver, USA. pp. 52.

Geoffroy, L., Callot, J.P., Aubourg, C., Moreira, M., 2002. Magnetic and plagioclase linear fabric discrepancy in dykes: a new way to define the flow vector using magnetic foliation. Terra Nova 14, 183–190.

Grégoire, V., de Saint Blanquat, M., Nédélec, A., Bouchez, J.L., 1995. Shape anisotropy versus magnetic interactions of magnetite grains: experiments and application to AMS in granitic rocks. Geophys. Res. Lett. 18, 2193–2196.

Grégoire, V., Darrozes, J., Gaillot, P., Nédélec, A., Launeau, P., 1998. Magnetite grain shape fabric and distribution anisotropy vs rock

magnetic fabric: a three-dimensional case study. J. Struct. Geol. 20, 937–944.
Hargraves, R.B., Johnson, D., Chan, C.Y., 1991. Distribution anisotropy: the cause of AMS igneous rocks? Geophys. Res. Lett. 18, 2193–2196.
Henry, B., Jordanova, D., Jordanova, N., Souque, C., Robion, P., 2003. Anisotropy of magnetic susceptibility of heated rocks. Tectonophysics 366, 241–258.
Herrero-Bervera, E., Cañón-Tapia, E., Walker, G.P.L., Tanaka, H., 2002. Magnetic fabrics study and inferred flow directions of lavas of the Old Pali Road, O'ahu, Hawaii. J. Volcanol. Geotherm. Res. 118, 161–171.
Ildefonse, B., Fernandez, A., 1988. Influence of the concentration of rigid markers in aviscous medium on the production or preferred orientations. An experimental contribution: 1. Non-coaxial strain. Bull. Geol. Inst. Univ. Upps., N.S. 14, 55–60.
Ildefonse, B., Mainprice, D., Gumão de Burgos, C.M., 2002. Crystallographic preferred orientations and seismic properties of gabbroic rocks. AGU meeting, San Francisco.
Jelinek, V., 1978. Statistical processing of magnetic susceptibility measured on groups of specimens. J. Geomagn. Geoelectr. 22, 50–62.
Jelinek, V., 1981. Characterization of the magnetic fabrics of rocks. Tectonophysics 79, 63–67.
Knight, M.D., Walker, P.L., 1988. Magma flow directions in dikes of the Koolau Complex, Oahu, determined from magnetic fabric studies. J. Geophys. Res. 93 (B5), 4301–4319.
Krieger Lassen, N.C., 1996. The relative precision of crystal orientations measured from electron backscattering patterns. J. Microsc. 181, 72–81.
Launeau, P., Cruden, A.R., 1998. Magmatic fabric acquisition mechanisms in a syenite: results of a combined anisotropy of magnetic susceptibility and image analysis study. J. Geophys. Res. 103 (B3), 5067–5089.
Launeau, P., Robin, P.-Y.F., 1996. Fabric analysis using the intercept method. Tectonophysics 267, 91–119.
Lloyd, G.E., Prior, D.J., 1999. EBSD technique and application in geosciences. Gött. Arb. Geol. Paläontol. Sb4, S112–S113.
Merle, O., 1998. Internal strain within lava flows from analogue modelling. J. Volcanol. Geotherm. Res. 81, 189–206.
Merle, O., 2000. Numerical modelling of strain lava tubes. Bull. Volcanol. 62, 53–58.
Moreira, M., Geoffroy, L., Pozzi, J.P., 1999. Écoulement magmatique dans les dykes du point chaud des Açores: étude préliminaire par anisotropie de susceptibilité magnétique (ASM) dans l'île de San Jorge. C. R. Acad. Sci., Paris 329, 15–22.
Nicolas, A., 1992. Kinematics in magmatic rocks with special reference to gabbros. J. Petrol. 33, 891–915.
Nishitani, T., 1981. Magnetic properties of titanomagnetites containing spinel (MgAl2O4). J. Geomagn. Geoelectr. 33 (B12), 171–179.
O'Reilly, W., 1984. Rock and Mineral Magnetism. Blackie, Glasgow. 230 pp.
Park, J.K., Tanczyk, E.I., Desbarats, A., 1988. Magnetic fabric and its significance in the 1400 Ma mealy diabase dykes of Labrador, Canada. J. Geophys. Res. 93 (B11), 13689–13704.
Pike, R.P., Roberts, A.P., Verosub, K.L., 1999. Characterizing interactions in fine magnetic particle systems using first order reversal curves. J. Appl. Phys. 85, 6660–6667.
Potter, D.K., Stephenson, A., 1988. Single domain particles in rocks and magnetic fabric analysis. Geophys. Res. Lett. 15, 1097–1100.
Roberts, A.P., Pike, R.P., Verosub, K.L., 2000. First-order reversal curve diagrams: a new tool for characterizing the magnetic properties of natural samples. J. Geophys. Res. 105 (B12), 28461–28475.
Rochette, P., Jackson, M., Aubourg, C., 1992. Rock magnetism and the interpretation of anisotropy of magnetic susceptibility. Rev. Geophys. 30, 209–226.
Rochette, P., Aubourg, C., Perrin, M., 1999. Is this magnetic fabric normal? A review and case studies in volcanic formations. Tectonophysics 307, 219–234.
Schmidt, N.H., Olesen, N.Ø., 1989. Computer-aided determination of crystal-lattice orientation from electron-channeling patterns in the SEM. Can. Mineral. 27, 15–22.
Senanayake, W.E., Mc Elhinny, M.W., 1982. The effects of heating on low-temperature susceptibility and hysteresis properties of basalts. Phys. Earth Planet. Inter. 30, 317–321.
Stephenson, A., 1994. Distribution anisotropy: two simple models for magnetic lineation and folation. Phys. Earth Planet. Inter. 82, 49–53.
Tarling, D.H., Hrouda, F., 1993. The Magnetic Anisotropy of Rocks. Chapman and Hall, London. 217 pp.
Ventura, G., De Rosa, R., Colleta, E., Mazzuoli, R., 1996. Deformation patterns in a high-viscosity lava flow inferred from the crystal preferred orientation and imbrication structures: an example from Salina (Aeolian Islands, southern Tyrrhenian Sea Italy). Bull. Volcanol. 57, 555–562.
Von Bonn, J.F., Heidelberg, H.J.L., 1965. Kalium-Argon-Daten zum Alter des Laacher Vulkanismus, der Rheinterrassen und der Eiszeiten. Eiszeitalt. Ggw. 16, 5–30.
Walker, G.P.L., Cañón-Tapia, E., Herrero-Bervera, E., 1999. Origin of vesicle layering and double imbrication by endogeneous growth in the Birkett basalt flow (Columbia river plateau). J. Volcanol. Geotherm. Res. 88, 15–28.
Wechsler, B.A., Lindsley, D.H., Prewitt, C.T., 1984. Crystal structure and cation distribution in titanomagnetite ($Fe_{3-x}Ti_xO4$). Am. Mineral. 69, 754–770.
Wenk, H.R., Joswig, W., Tagai, T., Korekawa, M., Smith, B.K., 1980. The average structure of An 62-66 labradorite. Am. Mineral. 65, 81–95.
Wolff, J.A., Ellwood, B.B., Sachs, S.D., 1989. Anisotropy of magnetic susceptibility in welded tuffs: application to a welded tuff dyke in the Tertiary Trans-Pecos, Texas volcanic province, USA. Bull. Volcanol. 51, 299–310.
Woodcock, N.H., Naylor, M.A., 1983. Randomless testing in three-dimensional orientation data. J. Struct. Geol. 5, 539–548.
Yaouancq, G., MacLeod, C.J., 2000. Petrofabric investigation of gabbros from the Oman ophiolite: comparison between AMS and rocks fabric. Mar. Geophys. Res. 21, 289–305.
Zhu, R., Shi, C., Liu, Q., 2003. Anisotropy of magnetic susceptibility of Hannuaoba basalt, northern China: constrain on the vent position of the lava sequences. Geophys. Res. Lett. 30 (38,1-38,4).